ACS OMEGA

Open Access

http://pubs.acs.org/journal/acsodf

Article

Laboratory Evaluation on the Water Flooding Characteristics in Bottom Water Reservoir Containing Interbeds

Pengfei Lee, Hong Tang,* Xianming Yan, Shaonan Zhang, Zhang Zhang, and Huafeng Liu

Cite This: *ACS Omega* 2023, 8, 42409−42416

Read Online

ACCESS | Metrics & More | Article Recommendations | Supporting Information

ABSTRACT: Sandstone reservoirs with bottom water drive are widely distributed all over the world, which are characterized by the complex process of oil and water storage and transmission. At present, the research on the water flooding process and oil−water evolution characteristics in bottom water reservoirs containing interbeds needs to be strengthened. In this study, water flooding experiments with different placements of the interbeds were conducted using a two-dimensional (2D) vertical model. The results demonstrated that the interbeds make the bottom water flow upward more evenly, resulting in decreased incursion speed, increased displacement area, and better displacement effect. Moreover, compared with the tilted interbed model, the horizontal model has a 6% higher oil recovery rate, exhibiting a better oil displacement effect. The results presented herein will provide important guidance on water control in bottom-aquifer oil reservoirs containing interbeds and will promote unconventional petroleum resources recovery.

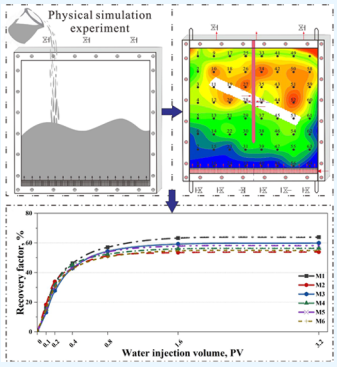

1. INTRODUCTION

Sandstone reservoirs with bottom water drive are important parts of unconventional petroleum resources, which are characterized by early water breakthrough, short water-free oil recovery period, rapid water cut increase, and strong heterogeneity.[1−5] With large scale and high abundance, bottom water reservoirs are strictly controlled by structure, stratum, and other conventional traps. Since natural interbeds between sandstone reservoirs and the bottom aquifer are usually weak or absent, water can easily intrude the production wells and the oil/water interface moves toward the wellbore.[6,7] Once water breakthrough occurs, the water cut increases significantly, which inhibits the flow of oil, and a large amount of residual oil remains in the middle and upper part of the reservoir, reducing production efficiency.[8−15] Therefore, the exploitation of sandstone reservoirs with bottom water drive suffers from the bottom water coning and huge production cost issues.[16−18]

An interbed is defined as a low permeability sublayer or an impervious stringer in a reservoir bed, such as sedimentogenic muddy intercalation, boulder clay, or diagenetic calcareous layer. In a bottom water drive reservoir, the low-permeability interbeds can prevent the injection water from flooding below the interbed where remaining oil can accumulate or decrease the flooding efficiency of the oil sheet above the interbeds due to their isolation effect.[19−21] The distribution of interbeds' feature can curb the occurrence of coning water effectively, which has a great influence on bottom water drive reservoir.[22,23] Therefore, it is of great scientific and engineering significance to systematically study the water flooding characteristics in the bottom water−oil reservoir containing interbeds. Wu et al.[4] investigated the mechanism of improved oil recovery by nitrogen foam flooding in bottom water reservoirs and revealed that the seepage resistance of foam in the water layer is much greater than that in the oil layer, effectively increasing the displacement strength of the oil layer. Liu et al.[7] used oil-soluble resin as selective water shut-off agent in artificial barriers and confirmed its important role in water control in low-permeability hydrocarbon reservoirs with bottom aquifers. Bai et al.[24] compared the production and decomposition dynamics of Class I hydrates with different patterns of interbeds by numerical simulation method and the results demonstrated that the cumulative gas production of hydrate can be reduced by 10% (the corresponding sealing degree is about 90%) when the mudstone interbed is whole interbed. Niu et al.[25] used a numerical method to investigate the hydromechanical coupling process of injecting fluid into subsurface reservoirs and found that the different locations of clayey interbeds in the reservoir have different impacts on the surface uplift. Zhou et al.[26] investigated the deformation characteristics of a laterally extensive lens-shaped clayey interbed in a sandstone aquifer during fluid injection by using cam clay and poroelastic theoretical models. The results confirmed that ground deformation due to the interbed can be classified into three-time intervals. Hu et al.[27] proposed the mathematical model of two-phase flow in the bottom water reservoir with the interbed,

Received: July 7, 2023
Revised: October 13, 2023
Accepted: October 18, 2023
Published: November 4, 2023

and analyzed the influence of the distribution of the interbeds on the water cut rising law of the bottom water reservoir. Yang et al.[28] investigated mechanisms and prevention& control countermeasures of water breakthrough in horizontal wells, and confirmed that the sealing capacity of the interbed increases with the decreases of its vertical permeability, and the increase of its shale content and thickness.

The present research on the distribution characteristics of oil and water in the bottom water−oil reservoir containing interbeds reveals certain limitations. First, the research on the influence of the interbed on the development of the bottom water reservoir mostly focuses on the experimental comparison of the macrodevelopment effect, and there is still a lack of research on its action mode. Second, studies related to water flooding characteristics under different combination conditions of "water-interbed-oil saturation" need to be strengthened; Third, further research is required to reveal the distribution mechanism of residual oil underlying the different interbed positions.

In this study, based on the reservoir characteristics of offshore Clastic rock heterogeneous reservoirs and the principle of similarity, two-dimensional plate oil displacement experiments were carried out with different interbed occurrences, and the water seepage characteristics of water in the oil layer and the distribution pattern for residual oil were summarized. The results presented herein will provide important guidance on water control in bottom water reservoirs containing interbeds and will promote the unconventional petroleum resources recovery.

2. EXPERIMENTAL SECTION

2.1. Apparatus. The apparatus mainly consists of a vacuum pump, a flat sand filling water displacement test system, an injection pump, a resistivity tester, a viscometer, a data acquisition system, etc. (Figure 1).

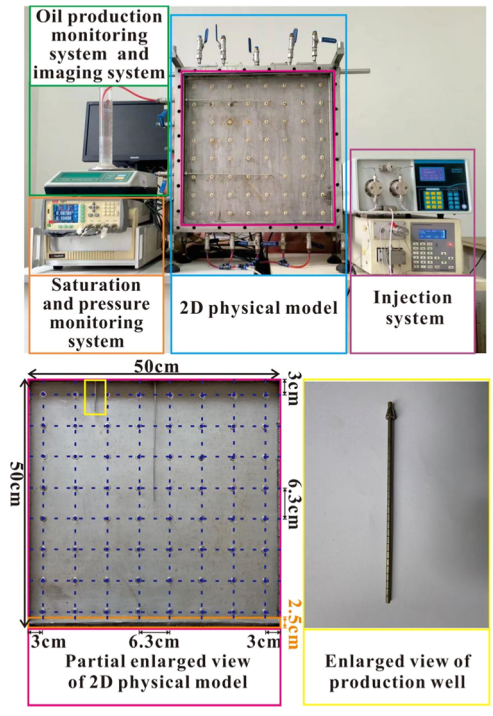

Figure 1. Drawing of experimental equipment and its local details.

The length, width, and height of the solid unit of the two-dimensional flat sand filling device is 50 cm × 50 cm × 3 cm, and the maximum pressure bearing capacity is 0.1 MPa (Figure 2). There are 64 equidistant electrodes arranged on the surface of the experimental device and connected with detection circuits to monitor the resistance parameters of the water-containing oil-sand reservoir in the device. The data of each electrode point is collected through the resistance data collector and aggregated into the LCR digital bridge instrument, and the experimental data are finally received and displayed by the computer. At the same time, 8 movable pressure detection points were flexibly placed on 64 electrode points to monitor their dynamic pressure in real time. The top and bottom of the experimental device are evenly arranged with 5 inlet and outlet valves, and each valve can be connected with the constant flow pump and can also be connected with the measuring device—measuring cylinder and electronic balance, to simulate the injection well during water injection and the production well during collection. At the same time, a low permeability horizontal partition board is installed at a position 2.5 cm from the bottom of the experimental device to simulate the bottom aquifer. The pressure of the bottom water remains constant during the experiment (Figure 1).

2.2. Interbed Experimental Models. Based on the reservoir characteristics of the Penglai 19−3 Oilfield, Bohai Bay, and hydrodynamics similar principles, reducing the proportion of a certain kind of model, the parameters for physical simulation experiments have been designed (Table 1).

The layout of the well pattern is a single model, which is designed according to the actual well network layout characteristics of Penglai 19−3 Oilfield, Bohai Bay. In offshore oil production, the well network density is small, the well spacing is large, and the single well control area is large. As compared with the well pattern, the influence of bottom water is more important in bottom water reservoirs, and the influence on each well is similar. Therefore, we chose the single well model to investigate the flooding characteristics of bottom water reservoirs. A stainless steel pipe is used to simulate the production well. Before filling the model, the pipe was fixed to the model opening with screws and connected to the external valve. At the same time, a layer of fine iron mesh was wrapped around the well to prevent plugging. The use of full well section shooting for oil production is because the same method is used for the oil production wells of the research oilfield. The permeability of the main oil layer in the research area is between 600 and 2200 mD. Using the principle of similarity, the reservoir permeability of the experimental models was designed to be 2000 mD. Moreover, by fully compacting with 40−60 mesh river sand, the reservoir permeability can be stabilized at around 2000 mD, which can be repeatedly and is convenient for comparison between these six sets of models.

Based on previous experience, the maximum extension width of the interbed is equivalent to 2/3 of the full bank width of the channel, and the inclination is between 3 and 25° (S1, Supporting Information). To enhance the shielding effect of the interbed, the angle of the interbed is set to 30°.

Six interbed experimental models were designed according to the presence or absence of interbeds, the dip angle (0, 30°) of interbeds, and the bottom hole position (low, high). The schematic diagram and characteristics of interbeds of the six experimental models are shown in Figure 3 and Table 2.

The interbed production mold of the interbed is a 35 cm × 3 cm × 3 cm cuboid, which is composed of 6 appropriately sized stainless steel plates. The interbed material is kaolin for scientific

https://doi.org/10.1021/acsomega.3c04873
ACS Omega 2023, 8, 42409−42416

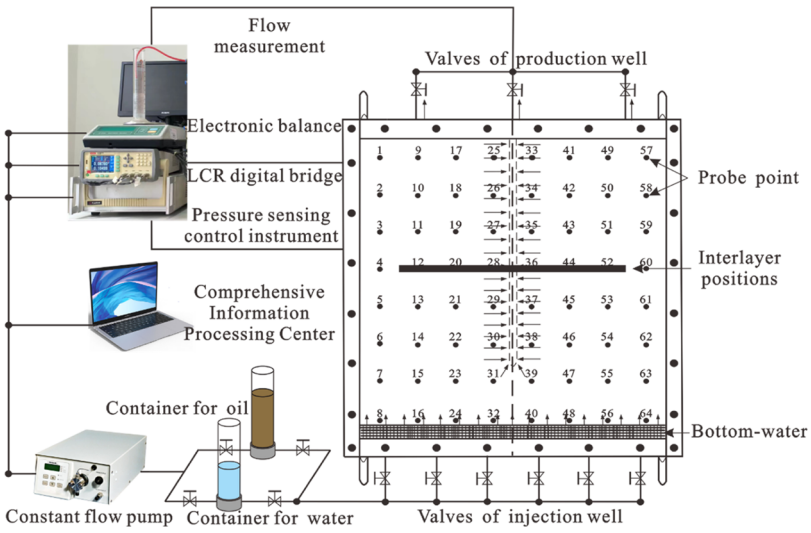

Figure 2. Experimental design for the seepage flow measurement.

Table 1. Physical Simulation Experiments and Prototype Parameters

parameter	porosity	permeability	oil viscosity	water viscosity	water density	oil density	daily injection volume
notation	Φ	K	μ_o	μ_w	e_0	e_w	q_f
unit	%	mD	mPa·s	mPa·s	g/cm^3	g/cm^3	m^3/d
oilfield parameters	18.9−34.7, average 27	600.0−2200.0, average 800	20	0.5	1	0.913−0.966	62−680
model design parameters	34	2000	40	1	1	0.8736	0.00864

experiments. The purity of kaolin is more than 98%, and the main impurity is Illite. The underwater particle size test results of kaolin were: D_{50} = 0.35 μm and D_{90} = 2.01 μm. Soak the kaolin in Ultrapure water and let it stand for 3−5 days. The solid kaolinite mud was obtained by removing the liquid on the surface. Cover a thin film in the cuboid's inner surface, which prevents the adhesion of kaolin. Press the Kaolinite mud into the cuboid. Let it stand for 12 h to remove water. The 4 interbeds were obtained by removing the six stainless steel plates of the production model. The interbed is 35 cm long, 3 cm wide, and 3 cm high. The interbed has poor permeability, high plasticity, and compressibility, and is not easy to crack in the process of sand filling.

2.3. Experimental Steps. The specific experimental steps are shown in Figure 4 and are described as follows:

2.3.1. Making a Sand Filling Model. The two-dimensional flat sand-filing device was first cleaned, and the monitoring device was checked. Subsequently, a layer of 100 mesh fine sand covered the surface of the model. The roughened surface prevented the boundary effect from being damaged, and cross-flow generated. River sand of 40−60 mesh was used to fill the model. The occurrence and location of the interbed were set in a proper way and buried in the production well section. Then, the sand was filled with a small amount of multiple ground, and the overall multiple vibration can make the sand body more densification. The "sand shake" was repeated several times to simulate the compaction process and reduce the pore volume between the sand particles so that it was spread as evenly as possible in the designed model.

2.3.2. Saturated Water Process. After the sand filling was completed, the experimental device was vacuumed as a whole, and then a constant flow pump was used to inject water into the model at a flow rate of 1 mL/min, continuously and evenly. After the resistance values of each electrode measured by the digital bridge instrument were stable, the water injection valve was closed, water injection was stopped, and the water injection process was repeated after the sand and gravel in the model were fully wetted. Finally, the total quality of the injected water was calculated. The model porosity was obtained, and the formation resistivity was then reset.

The six experimental models used in this experiment had a maximum porosity of 38.45%, a minimum porosity of 34.26%, and an average porosity of 36.35% (Table 3). The maximum permeability was 2687 mD, the minimum was 1926 mD, and the average permeability was 2254.9 mD. The error between the models was small, and it was more consistent with the actual physical characteristics of the Miocene formation of the Tertiary in the study area; therefore, it was suitable to carry out simulation experiments.

2.3.3. Saturated Oil Process. First, the quality of the oil to be injected was weighed, the valve of the top water injection port was opened, and the constant flow pump was used to inject water into the model at a flow rate of 1 mL/min. After the bottom water injection port was completely discharged (without water) for a period of time, the valve was closed, the oil injection was stopped, and the oil injection process was repeated after the oil and water in the model were stratified again. Finally, the total injected oil mass and produced water mass in the device were calculated, the bound water mass was calculated, and the oil saturation and bound water saturation in the device were obtained.

2.3.4. Water Displacement Process. After the flow rate of the constant flow pump was set to 1 mL/min, the valve at the bottom of the water injection port was opened to start the water injection displacement process. The resistivity and pressure data of each electrode were measured by the digital bridge instrument and pressure monitoring device monitor. 64 electrode points were scanned every 13 s on average to generate, and the

https://doi.org/10.1021/acsomega.3c04873
ACS Omega 2023, 8, 42409−42416

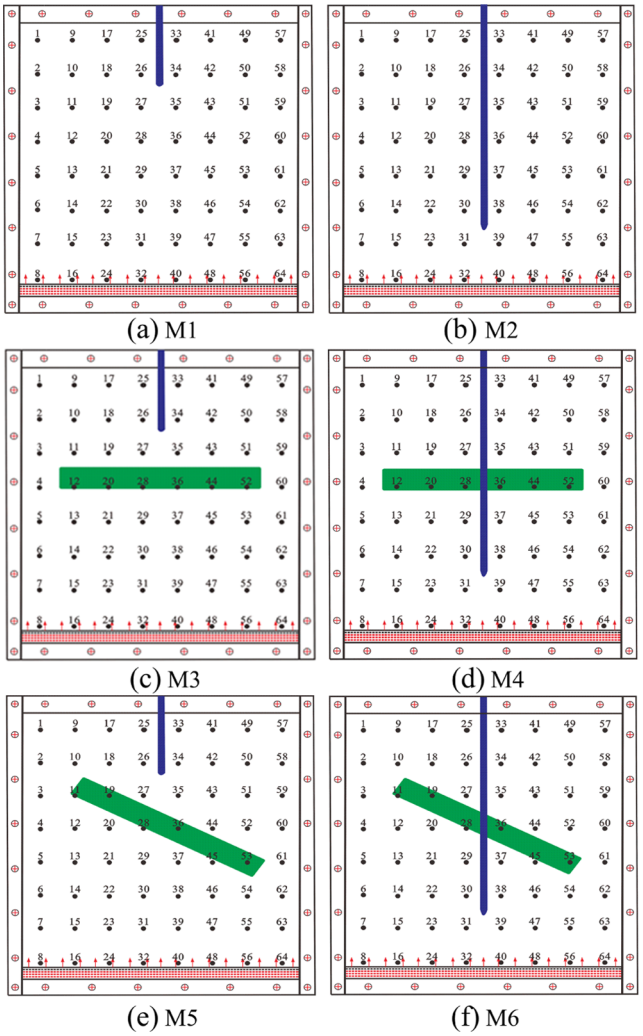

Figure 3. Schematic diagram of the interbed experimental models. The green area denotes the interbed. (a) High well location homogeneous model. (b) Low well location homogeneous model. (c) High well location with horizontal interbed. (d) Low well location with horizontal interbed. (e) High well location tilted interbed. (f) Low well location tilted interbed.

Table 2. Interbed Experimental Model

model no.	characteristics of interbeds	perforated positions
M1	homogeneous models (without interbed)	high well position (12.5 cm away from the top surface)
M2		low well position (37.5 cm away from the top surface)
M3	horizontal interbed models (0°)	high well position (12.5 cm away from the top surface)
M4		low well position (37.5 cm away from the top surface)
M5	tilted interbed models (30°)	high well position (12.5 cm away from the top surface)
M6		low well position (37.5 cm away from the top surface)

resistivity planar distribution was record The changes of the bottom water front were observed at different injected water volume (PV number) time nodes. Continue flooding until the stage water cut reached about 99% and the resistance was basically stable. The produced oil and water quality and recovery rates under different injected water volumes were calculated.

2.3.5. Data Processing. The measured resistivity was converted into the oil saturation near the electrode in the model by using Archie's equation, which has been accepted as an industry standard to determine water saturation and widely used in well-log interpretations for the fluid saturation calculation from electrical resistivity measurement.[29−31]

$$S_w = \sqrt[n]{\frac{abR_w}{\varphi^m R_t}} \quad (1)$$

where S_w is the water saturation of an electrode in models; R_w and R_t are the resistivity of water and liquid sand body in the experiment, respectively; ϕ is the porosity; a, b, m, and n are the lithologic parameter, lithology index, cementation coefficient, and saturation index, respectively, whose values are taken as 1, 1, 2, and 2, respectively. The oil saturation distribution map of the model was made with mapping software.

3. RESULTS AND DISCUSSION

3.1. Flooding Performance of Bottom Water Reservoir Models Containing Interbeds. The flooding results for the six displacement models are summarized in Table 4.

Figure 5a gives the experimental results about pressure vs the water injection volume (PV number). As shown in Figure 5a, the displacement pressure of each model increases sharply with the progress of water flooding, which can be ascribed to the high capillary pressure in the cone. The displacement pressure rapidly decreases and gradually stabilizes with the formation of a breakthrough by the injected water.

Figure 5b shows the diagram of the relationship between the stage water cut and water injection volume of each model, which has a period of anhydrous oil recovery before the breakthrough of injected water. Once a breakthrough is formed, its instantaneous water content increases sharply, reaching over 60% at 0.8 PV, and the displacement effect weakens and stabilizes at around 98%.

As compared with the high well location models (M1; M3; M5), the low well position models (M2; M4; M6) have a relatively short water-free oil recovery period and have already formed breakthroughs before 0.2 PV. The above results indicate that the high well location models can effectively increase the time for anhydrous oil recovery.

Figure 5c shows a diagram of the relationship between the recovery factor and water injection volume of each model. At the initial stage of oil production, the recovery rate reaches over 13% when the injection water is only 0.1 PV. However, within 0.4 PV, the recovery rate can all be above 42%. At 0.8 PV, it can reach 90% of the oil production, and after 1.6 PV, the oil production has hardly increased. M3 has the highest recovery ratio at water breakthrough, indicating that the horizontal interbed plays a significant role in suppressing the bottom water coning.

3.2. Distribution Characteristics of Remaining Oil Saturation after Flooding. The distribution map of oil saturation in the water flooding experiment is shown in Figure 6 and the distribution characteristics of remaining oil saturation for different flooding models (M1−M6) are analyzed as follows:

3.2.1. Homogeneous Flooding Model. A large area of low residual oil saturation area appears in the low part of M1, indicating that M1 has the best oil displacement effect in the low part of the sand body. It was obvious that in the high permeability sand body in the M1, the water flooding performance exhibited smooth spread, as shown in Figure 6(a). The significant bottom water coning phenomenon in the

https://doi.org/10.1021/acsomega.3c04873
ACS Omega 2023, 8, 42409−42416

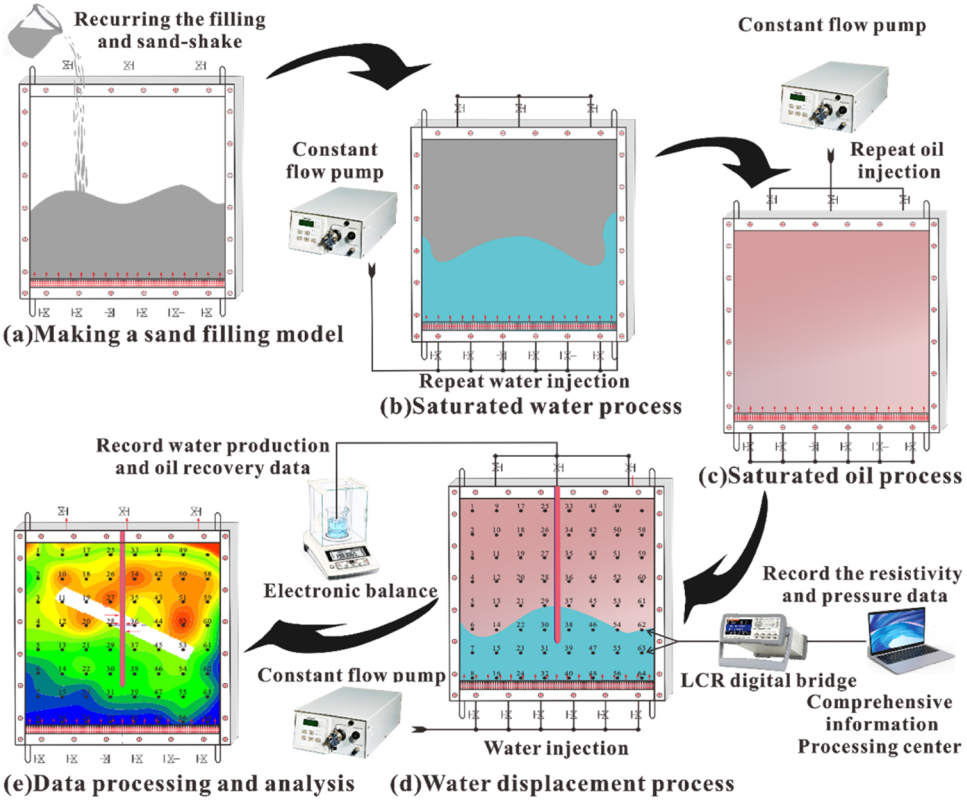

Figure 4. Experimental process roadmap. (a) Making a sand filling model. (b) Saturated water process. (c) Saturated oil process. (d) Water displacement process. (e) Data processing.

Table 3. Statistical Data of Physical Properties in Six Experimental Models (Flow Velocity is 1 mL/min)

model no.	M1	M2	M3	M4	M5	M6	average value
permeability (mD)	2687	2479	1926	1992	2246	2213	2254.9
porosity (%)	38.45	37.69	34.26	34.78	35.70	35.20	36.02

Table 4. Statistical Data of Physical Properties in Experimental Models (Flow Velocity is 1 mL/min)

model no.	water injection volume, PV	0	0.1	0.2	0.4	0.8	1.6	3.2
M1	stage water cut, %	0	0	0	30.8	67.7	92.8	98.8
	recovery rate, %	0	16.2	32.8	46.3	57.1	63.3	63.7
M2	stage water cut, %	0	0	15	48.9	77.6	93.5	99.3
	recovery rate, %	0	18.3	33.9	43.1	51.2	53.5	53.9
M3	stage water cut, %	0	0	0	0	61.2	91.9	98.8
	recovery rate, %	0	13.1	27.8	42.9	56.4	60.5	61
M4	stage water cut, %	0	0	7.9	41.6	75.8	94	99.1
	recovery rate, %	0	15.3	31.5	45.2	54.4	58.0	58.4
M5	stage water cut, %	0	0	0	13	68.1	93.1	98.5
	recovery rate, %	0	14.6	30.2	43.3	52.7	55.3	55.6
M6	stage water cut, %	0	0	12.1	47.1	76.3	94.6	98.9
	recovery rate, %	0	15	29.8	42.5	50.0	52.1	52.4

bottom area of Model 2 results in a large area of the remaining oil in the upper area. Due to the fact that the well location is close to the bottom of the model, the phenomenon of bottom water coning is obvious in M2 (Figure 6b).

3.2.2. Heterogeneous Flooding Models with Horizontal Interbeds. M3 has the highest recovery ratio at water breakthrough and has the largest swept area, and most areas in the M3 have better oil displacement efficiency. It can be seen from the distribution map of remaining oil saturation (Figure 6c) that the bottom water coning in M3 is significantly inhibited. M4 has a phenomenon of bottom water coning, resulting in a large area of remaining oil in the upper area of the interbed; There is a small area of remaining oil in the middle of the upper part of the interbed, and the displacement effect of the lower part of the horizontal interbed in Model 4 is relatively good, with no obvious bottom water coning (Figure 6d). However, the displacement effect of the upper part of the interbed is relatively poor, and there is residual oil in the middle position of the upper. According to the hydrodynamics continuity equation, when the injected water quantity is unchanged, that is, the flow rate is unchanged, the narrowing of the flow channel will inevitably lead to the increase of flow velocity, that is, the increase of kinetic

https://doi.org/10.1021/acsomega.3c04873
ACS Omega 2023, 8, 42409−42416

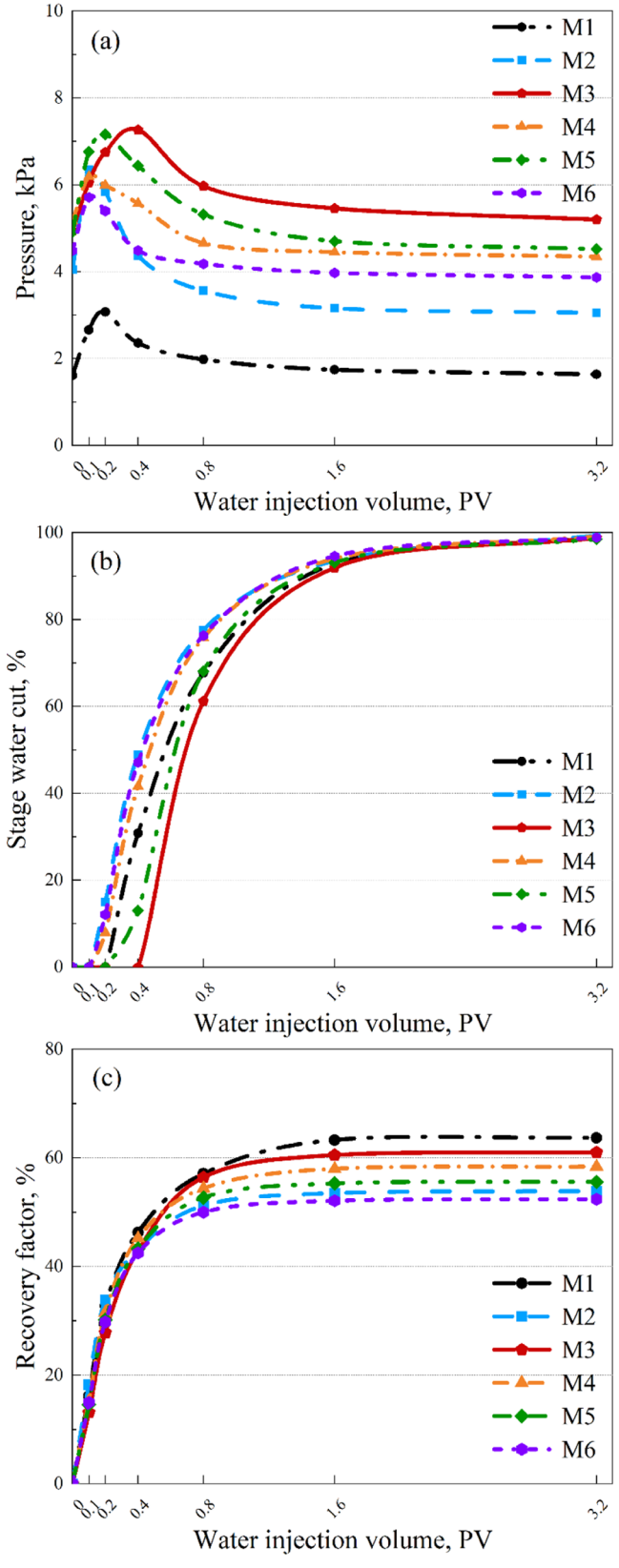

Figure 5. Diagrams of the relationship between (a) pressure with water injection volume of each model. (b) Stage water cut with water injection volume of each model. (c) Recovery factor with water injection volume of each model.

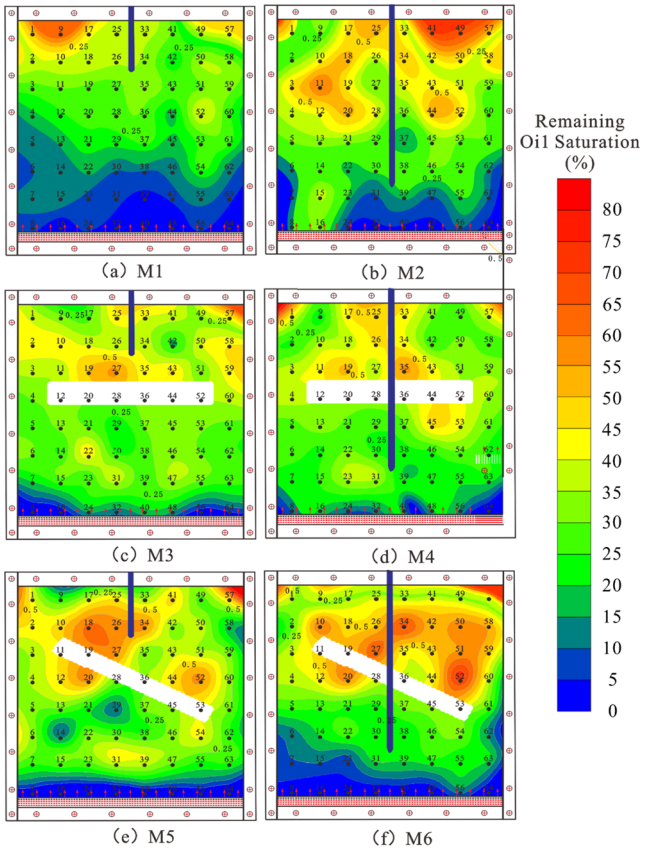

Figure 6. Remaining oil saturation distribution in water flooding experiment for different models (M1−M6).

energy of the fluid; otherwise, the flow velocity will decrease after passing the channel. According to the law of energy conservation of hydrodynamics, on the same flow line, when it flows upward through the channel, its kinetic energy decreases and its pressure energy decreases, which will inevitably lead to an increase in potential energy, resulting in the preferential movement of injected water to the upper part of the model after passing through the interbed, rather than moving along the shortest migration path. At the same time, both fluid velocity and momentum are vectors, and both have the ability to maintain their inherent direction (upward). This is the reason why this area is the largest remaining oil-rich area.

The above results indicate that the horizontal interbed plays a significant role in suppressing the bottom water coning.

3.2.3. Heterogeneous Flooding Models with Inclined Interbeds. It can be seen that the bottom water coning is significantly suppressed in M5 (Figure 6e) and most of the injected water advanced along the downdip direction of the tilted interbed, resulting in a large area of remaining oil in the upward inclination direction of the interbed. A slight bottom water coning phenomenon was also observed in M6 (Figure 6f) and there is a water drive advantage channel along the downdip direction of the tilted interbed. It resulted in a large area of remaining oil in the upper part of the model. Compared with the M3 and M4 models, the M5 and M6 models have a larger range of remaining oil in the upper part of the interbed. Therefore, the tilted interbed has a greater shielding effect than the horizontal interbed. This is conducive to the formation of dominant migration channels in the downdip direction of the interbed and the rapid breakthrough of injected water.

From the final remaining oil distribution map of remaining oil in different models, it can be observed that the presence of

https://doi.org/10.1021/acsomega.3c04873
ACS Omega 2023, 8, 42409−42416

interbed makes the bottom water advance more evenly, slows down the trusting speed, and increases the swept area, achieving a good displacement effect.

4. CONCLUSIONS

In this work, we take the water flooding mechanism in bottom water−oil reservoirs as the research object, and systematically investigate the water flooding mechanisms of bottom water reservoirs containing interbeds, and some interesting points are obtained:

(1) In the development of bottom water reservoirs, the best flooding effect is achieved by perforating near the top of the sand body, especially above relatively large interbeds, the recovery rate can even be increased by 10%.
(2) Both horizontal and tilted interbeds have a certain shielding effect on the bottom water, effectively suppressing the coning of the bottom water. The presence of interbeds making the upward movement of bottom water more uniform in the lower area of the interbed, slowing down the thrusting speed, increasing the sweep area, and achieving better displacement effects.
(3) By comparing the development effects of the horizontal interbed model and the tilted interbed model, it was found that the tilted model has a stronger occlusion effect. However, the tilted interbed model is more likely to form dominant seepage channels. This is conducive to the rapid breakthrough of injected water, resulting in more areas with poor spread and the formation of larger residual oil. Therefore, its development effect is the worst. Compared to the horizontal interbed model, its recovery rate is about 6% less.
(4) The preferential movement of bottom water to the upper part of the model after passing through the interbed, rather than moving along the shortest migration path. This is the reason why the middle position of the upper area is the largest remaining oil-rich area.

■ ASSOCIATED CONTENT

Supporting Information

The Supporting Information is available free of charge at https://pubs.acs.org/doi/10.1021/acsomega.3c04873.

Setting of parameters for physical simulation experiments and distribution table of interbeds inclination angle (PDF)

■ AUTHOR INFORMATION

Corresponding Author

Hong Tang − *School of Geoscience and Technology, Southwest Petroleum University, Chengdu, Sichuan 610500, China;* orcid.org/0009-0009-2447-233X; Email: tangh@swpu.edu.cn

Authors

Pengfei Lee − *School of Geoscience and Technology, Southwest Petroleum University, Chengdu, Sichuan 610500, China*

Xianming Yan − *Ziyang Branch, Shaanxi City Gas Industry Development Co., Ltd., Ziyang, Shaanxi 725300, China*

Shaonan Zhang − *School of Geoscience and Technology, Southwest Petroleum University, Chengdu, Sichuan 610500, China*

Zhang Zhang − *Tianjin Branch, CNOOC China Limited, Tianjin 300452, China*

Huafeng Liu − *School of Geoscience and Technology, Southwest Petroleum University, Chengdu, Sichuan 610500, China*

Complete contact information is available at: https://pubs.acs.org/10.1021/acsomega.3c04873

Author Contributions

H.T.: methodology, writing review and editing. P.L.: experiments, data curation, drawing, visualization, formal analysis, writing−original draft and revisions. X.Y.: experiments, data curation, and drawing. Z.S.: methodology, writing review and editing. Z.Z.: investigation, writing−review and editing. H.L.: experiments and data curation.

Notes

The authors declare no competing financial interest.

■ ACKNOWLEDGMENTS

The authors are grateful for the financial support by the Major Projects of National Science and Technology (2016ZX05058-006) and the State Key Laboratory Fund for Oil and Gas Reservoir Geology and Development Engineering (PLN1521).

■ REFERENCES

(1) Wang, W.; Tan, J.; Mu, S.; Li, B.; Zhang, W. Study on Flow Unit of Heavy Oil Bottom Water Reservoir with Over-Limited Thickness in Offshore Oilfield. *Open J. Geol.* **2019**, *09*, 507−515.

(2) Zuhair, A.; Subhash, A.; Ayrat, G.; Sunil, K. Evaluating foam stability using tailored water chemistry for gas mobility control applications. *J. Pet. Sci. Eng.* **2020**, *195*, No. 107532.

(3) Liao, H.; Xu, T.; Yu, H. Progress and prospects of EOR technology in deep, massive sandstone reservoirs with a strong bottom-water drive. *Energy Geosci.* **2023**, *28*, No. 100164.

(4) Wu, Y.; Zhang, Y.; Wang, J.; Ma, Y.; Song, Z.; Zeng, X.; Cao, A. Study on the mechanism of improved oil recovery by nitrogen foam flooding in bottom water reservoirs. *Front. Energy Res.* **2023**, *11*, No. 1120635.

(5) Su, X.; Qi, N.; Shi, X.; Zhang, Z.; Zhang, Z.; Luo, P.; Yu, Z. Feasibility of foamed acid treatment in upper stimulation of fractured-vuggy dolomite reservoirs with bottom water. *Geoenergy Sci. Eng.* **2023**, *224*, No. 211552.

(6) Liu, D.; Liu, Y.; Lai, N.; Hu, T.; Pang, Z.; Liu, T. Integrating Physical and Numerical Simulation of Horizontal Well Steam Flooding in a Heavy Oil Reservoir. *J. Energy Resour. Technol.* **2023**, *145*, No. 062601.

(7) Liu, K.; Zhu, W.; Pan, B. Laboratory evaluation on oil-soluble resin as selective water shut-off agent in water control fracturing for low-permeability hydrocarbon reservoirs with bottom aquifer. *Geoenergy Sci. Eng.* **2023**, *225*, No. 211672.

(8) You, Q.; Wen, Q.; Fang, J.; Guo, M.; Zhang, Qi.; Dai, C. Experimental study on lateral flooding for enhanced oil recovery in bottom-water reservoir with high water cut. *J. Pet. Sci. Eng.* **2019**, *174*, 747−756.

(9) Jiang, Q.; Chao, J.; Wang, Z.; Jia, N.; Kong, C.; Chang, T.; Liu, K.; He, L.; Li, T. Visualized Experimental Study of Nitrogen Injection Supression of Bottom Water Coning. *Chem. Technol. Fuels Oils* **2020**, *56*, 453−464.

(10) Wang, H.; Liu, Y. Horizontal Well Completion with Multiple Artificial Bottom Holes Improves Production Performance in Bottom Water Reservoir. *Math. Probl. Eng.* **2020**, *2020*, No. 7247480.

(11) Zoeir, A.; Simjoo, M.; Chahardowli, M.; Hosseini-Nasab, M. Foam EOR performance in homogeneous porous media: simulation versus experiments. *J. Pet. Explor. Prod. Technol.* **2020**, *10*, 2045−2054.

(12) Li, S.; Liu, Y.; Xue, L.; Yang, L.; Yuan, Z.; Jian, C. An investigation on water flooding performance and pattern of porous carbonate reservoirs with bottom water. *J. Pet. Sci. Eng.* **2021**, *200*, No. 108353.

(13) Chen, D.; Zhao, H.; Liu, K.; Huang, Y.; Li, B. The effect of emulsion and foam on anti-water coning during nitrogen foam injection in bottom-water reservoirs. *J. Pet. Sci. Eng.* **2021**, *196*, No. 107766.
(14) Wang, K.; Tang, C.; Zhang, T.; Gao, Y.; Zou, J.; Jiang, Y.; Sun, K.; Chen, Y. Theoretical Research on the Movement Law of Water Cone Behavior in Heavy Oil Reservoirs with Bottom Water. *Geofluids* **2022**, *2022*, No. 2954973.
(15) Anbari, H.; Robinson, J. P.; Greaves, M.; Rigby, S. P. Field performance and numerical simulation study on the toe to heel air injection (THAI) process in a heavy oil reservoir with bottom water. *J. Pet. Sci. Eng.* **2023**, *220*, No. 111202.
(16) Huang, X.; Guo, X.; Zhou, X.; Shen, C.; Lu, X.; Qi, Z.; Xiao, Q.; Yan, W. Effects of water invasion law on gas wells in high temperature and high pressure gas reservoir with a large accumulation of water-soluble gas. *J. Nat. Gas Sci. Eng.* **2019**, *62*, 68−78.
(17) Kai, W.; Wensheng, Z.; Ke, L.; Chen, L.; Yanhong, G.; Yue, P.; Gefeng, P.; Qing, Y. Study on Water Cone Behavior in Heavy Oil Reservoir with Bottom Water through Numerical Simulation. *Energy Sources, Part A* **2020**, *42*, 1809−1820.
(18) Kumar, M.; Sharma, P.; Gupta, D. K. Optimization of vertical well completion in a saturated reservoir with bottom water drive for maximizing recovery. *Biofuels* **2019**, *10*, 373−384.
(19) Tran, T. V.; Truong, T. A.; Ngo, A. T.; Hoang, S. K.; Trinh, V. X. A case study of gas-condensate reservoir performance under bottom water drive mechanism. *J. Pet. Explor. Prod. Technol.* **2019**, *9*, 525−541.
(20) Hu, J.; Li, A.; Memon, A. Experimental Investigation of Polymer Enhanced Oil Recovery under Different Injection Modes. *ACS Omega* **2020**, *5*, 31069−31075.
(21) Hu, J.; Li, A. Experimental Investigation of Factors Influencing Remaining Oil Distribution under Water Flooding in a 2-D Visualized Cross-Section Model. *ACS Omega* **2021**, *6*, 15572−15579.
(22) Fu, Y. A critical productivity equation of horizontal wells in a bottom water drive reservoir with low-permeability interbeds. *Arabian J. Geosci.* **2019**, *12*, No. 758.
(23) Sharma, P.; Kumar, M.; Gupta, D. K. 3D numerical simulation of clastic reservoir with bottom water drive using various ior techniques for maximizing recovery. *J. Pet. Explor. Prod. Technol.* **2019**, *9*, 1075−1087.
(24) Bai, Y.; Hou, J.; Liu, Y.; Lu, N.; Zhao, E.; Ji, Y. Interbed patterns division and its effect on production performance for class I hydrate deposit with mudstone interbed. *Energy* **2020**, *211*, No. 118666.
(25) Niu, Z.; Li, Q.; Wei, X. Estimation of the surface uplift due to fluid injection into a reservoir with a clayey interbed. *Comput. Geotech.* **2017**, *87*, 198−211.
(26) Zhou, X.; Burbey, T. J. Deformation characteristics of a clayey interbed during fluid injection. *Eng. Geol.* **2014**, *183*, 185−192.
(27) Hu, Y.; Zhang, X.; Ding, W.; Cheng, Z.; Qu, Lo.; Su, P.; Sun, C.; Zhang, W. The Effect of Interlayer on Water Cut Rise in a Bottom Water Reservoir. *Geofluids* **2021**, *2021*, No. 5558719.
(28) Yang, Y.; Gu, D.; Lian, Y.; Liu, G.; Han, S.; Chang, L.; Ma, Y.; Zhang, Y. Mechanisms and prevention & control countermeasures of water breakthrough in horizontal wells in multi-layer unconsolidated sandstone gas reservoirs; A case study of the Tainan Gas Field in the Qaidam Basin. *Nat. Gas Ind. B* **2019**, *6*, 564−571.
(29) Zhong, Z.; Rezaee, R.; Esteban, L.; Josh, M.; Feng, R. Determination of Archie's cementation exponent for shale reservoirs; an experimental approach. *J. Pet. Sci. Eng.* **2021**, *201*, No. 108527.
(30) Jin, Y.; Li, S.; Yang, D. Experimental and theoretical quantification of the relationship between electrical resistivity and hydrate saturation in porous media. *Fuel* **2020**, *269*, No. 117378, DOI: 10.1016/j.fuel.2020.117378.
(31) Nazemi, M.; Tavakoli, V.; Sharifi-Yazdi, M.; Rahimpour-Bonab, H.; Hosseini, M. The impact of micro-to macro-scale geological attributes on Archie's exponents, an example from Permian−Triassic carbonate reservoirs of the central Persian Gulf. *Mar. Pet. Geol.* **2019**, *102*, 775−785.

https://doi.org/10.1021/acsomega.3c04873
ACS Omega 2023, 8, 42409−42416